Jyväskylän yliopiston julkaisuarkisto
Jyväskylä University Digital Archive

UNIVERSITY OF JYVÄSKYLÄ

This is an electronic reprint of the original article.
This reprint *may differ* from the original in pagination and typographic detail.

Author(s): Leppänen, Teemu; Erkkilä, Anna-Leena; Kouko, Jarmo; Laine, Valtteri; Sorvari, Joonas

Title: A plasticity model for predicting the rheological behavior of paperboard

Year: 2017

Version:

Please cite the original version:

Leppänen, T., Erkkilä, A.-L., Kouko, J., Laine, V., & Sorvari, J. (2017). A plasticity model for predicting the rheological behavior of paperboard. International Journal of Solids and Structures, 106-107, 38-45. https://doi.org/10.1016/j.ijsolstr.2016.11.033

All material supplied via JYX is protected by copyright and other intellectual property rights, and duplication or sale of all or part of any of the repository collections is not permitted, except that material may be duplicated by you for your research use or educational purposes in electronic or print form. You must obtain permission for any other use. Electronic or print copies may not be offered, whether for sale or otherwise to anyone who is not an authorised user.

Accepted Manuscript

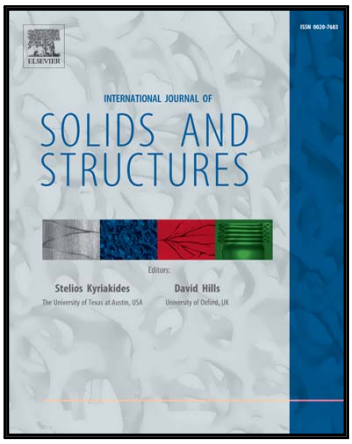

A plasticity model for predicting the rheological behavior of paperboard

Teemu Leppänen, Anna-Leena Erkkilä, Jarmo Kouko, Valtteri Laine, Joonas Sorvari

PII: S0020-7683(16)30367-5
DOI: 10.1016/j.ijsolstr.2016.11.033
Reference: SAS 9386

To appear in: *International Journal of Solids and Structures*

Received date: 1 August 2016
Revised date: 23 November 2016
Accepted date: 30 November 2016

Please cite this article as: Teemu Leppänen, Anna-Leena Erkkilä, Jarmo Kouko, Valtteri Laine, Joonas Sorvari, A plasticity model for predicting the rheological behavior of paperboard, *International Journal of Solids and Structures* (2016), doi: 10.1016/j.ijsolstr.2016.11.033

This is a PDF file of an unedited manuscript that has been accepted for publication. As a service to our customers we are providing this early version of the manuscript. The manuscript will undergo copyediting, typesetting, and review of the resulting proof before it is published in its final form. Please note that during the production process errors may be discovered which could affect the content, and all legal disclaimers that apply to the journal pertain.

ACCEPTED MANUSCRIPT

A plasticity model for predicting the rheological behavior of paperboard

Teemu Leppänen[a,*], Anna-Leena Erkkilä[b], Jarmo Kouko[c], Valtteri Laine[a], Joonas Sorvari[d]

[a] *LUT Savo Sustainable Technologies, Lappeenranta University of Technology, Varkaus unit, Opiskelijankatu 3, FI-78210 Varkaus, Finland*
[b] *University of Jyväskylä, PO Box 35, FI-40014 Jyväskylä, Finland*
[c] *VTT Technical Research Centre of Finland Ltd, PO Box 1603, FI-40101 Jyväskylä, Finland*
[d] *Centre of Computational Engineering and Integrated Design (CEID), Lappeenranta University of Technology, PO Box 20, Lappeenranta, FI-53851, Finland*

Abstract

The sorption of water into the paperboard exposes a container to reversible and irreversible deformations under relative humidity variations. In this study, an elasto-plastic material model is used to demonstrate how through-thickness dry solids content gradients can generate permanent in-plane strains in paperboard. The measurements presented in this paper indicate that in consecutive loading-unloading cycles, the yield stress either remains roughly constant or decreases, and an additional permanent set of strain is obtained even when the maximum tension of repetitions stays constant. Two modified approaches concerning elasto-plastic hardening behavior based on the measurements of this work and the observations of previous studies are introduced. The simulated results exhibit some shared features of the frequently observed shrinkage behavior of paperboard exposed to cyclic

*Corresponding author. Tel.: +358 50 439 4912
Email address: teemu.leppanen@lut.fi (Teemu Leppänen)

ACCEPTED MANUSCRIPT

ACCEPTED MANUSCRIPT

relative humidity changes. The results suggest that with the use of a suitable hardening approach, the plastic deformations arising from through-thickness dry solids content gradients may be considered as a time-independent component for simulations of phenomena such as moisture-accelerated creep and release of dried-in stresses.

Keywords: Paperboard, Moisture-accelerated creep, Mechano-sorptive creep, Elasto-plasticity, Dry solids content gradient, Cyclic humidity changes

1. Introduction

The rheological behavior of paperboard is connected to phenomena such as stress relaxation (Craven (1962)), strain recovery and moisture-accelerated creep. All these are important factors affecting paperboard production, converting and end-use quality. The potential of paperboard-based packages to resist a buckling collapse under a compressive load in relative humidity (RH) fluctuations during long-term storage or shipping is an important aspect of the performance of corrugated containers.

The sorption of water into the paperboard exposes the container to hygroexpansion and changes in mechanical properties and internal stresses. Depending on the drying history, the deformations arising under cyclic RH conditions may manifest irreversible behavior (Uesaka et al. (1992); Nanri and Uesaka (1993)). Long compressive loading times increase the risk for collapse due to creep. Moisture-accelerated creep, also known as mechano-sorptive creep, is a phenomenon in which the cyclic dry solids content (DSC = kg dry solids/(kg dry solids + kg water)×100%) changes increase the creep

ACCEPTED MANUSCRIPT

rate in paperboard. This creep rate increases with lower DSC levels, and because of the cyclic DSC changes, the creep rate is usually even higher than it would be at any constant DSC level (Byrd and Koning (1978); Leake and Wojcik (1992); Coffin (2005)). Delayed recovery is also a rheological property of paperboard. Elastic recovery immediately follows the stress-strain cycle, but after this, the strain continues to decrease under zero-loading conditions as a delayed strain recovery (Gates and Kenworthy (1963); Skowronski and Robertson (1986)).

Orthotropic elasto-plastic approaches to predict the in-plane tensile response and deformation of paper have been applied by Castro and Ostoja-Starzewski (2003), Mäkelä and Östlund (2003) and Xia et al. (2002). The effect of pre-straining on the yield surface has been modeled by Borgqvist et al. (2014). The behavior of paperboard and corrugated cardboard under cyclic loading has been studied by Allaoui et al. (2009). The effect of local material variations on out-of-plane deformations has been studied by Lipponen et al. (2008) and Erkkilä et al. (2015). Hygroviscoelastic models for predicting history-dependent dimensional stability and hygroexpansivity have been introduced by Uesaka et al. (1989) and Lif (2006). A model capturing several phenomena has been presented by Coffin (2009) and the effect of pre-straining on the tensile response of paper by using an efficiency factor has been studied in Coffin (2012). For decades, several macro- and micro-scale explanations have been proposed to describe the phenomena related to moisture-accelerated creep. Habeger and Coffin (2000) have considered the effect of DSC gradients and the related through-thickness stress distributions on the moisture-accelerated creep. The effect of hygroexpansion

ACCEPTED MANUSCRIPT

on creep behavior has also been considered by Urbanik (1995) and Haslach (1994). Alfthan et al. (2002) and Alfthan (2003) have demonstrated that nonlinear creep behavior of the material combined with the moisture gradients occurring during DSC changes and the potential material inhomogeneities may cause stresses inducing the moisture-accelerated creep. Samples of very low basis weight was used by Alfthan (2004) to minimize the effect of through-thickness DSC gradients. A micro-scale modeling approach has also been used by Strömbro and Gudmundson (2008a) and Strömbro and Gudmundson (2008b) to investigate the effects of different parameters on the moisture-accelerated creep. Vlahinić et al. (2012) have suggested that the viscous softening and both the basic and moisture-accelerated creep are mainly originating from the nanoscale movement of water which enhances the internal lubrication. Padanyi (1993) has proposed that aging is a parameter as important as temperature and relative humidity for creep and in Padanyi (1991) has been concluded that physical aging and mechano-sorptive effects are actually the same phenomenon. In Reichel and Kaliske (2015a) and Reichel and Kaliske (2015b) a 3D model for wooden structures demonstrating linear viscoelastic and non-linear viscoelastic-viscoplastic material behavior have been presented. The accumulated mechano-sorptive deformations were considered as amplification of mechanically induced creep.

The purpose of the present study is to estimate the potential of time-independent elasto-plastic hardening simulations to generate permanent deformations arising from the through-thickness DSC gradients. The basic concept is same as in the simple theoretical two bar model presented by Selway and Kirkpatrick (1992). The theoretical approach is extended by a

ACCEPTED MANUSCRIPT

material model describing the elasto-plastic behavior of paperboard. In addition to the traditional approach, the hardening behavior arising from DSC cycling is dealt with using two modified approaches based on observations in Östlund et al. (2004) and Nanri and Uesaka (1993) and the measurements introduced in this work. The results of the simulations are discussed with reference to previously published results related to the moisture-accelerated creep and the internal stresses. The results suggest that the accumulation of the plastic strains may have significant role in the phenomena arising in cyclic humidity conditions. The simulations also address the importance of the hardening behavior under cyclic loadings.

2. Measurements

The tensile behavior in the cross-machine direction (CD) (see Fig. 1) of an unbleached semi-chemical board sample with a basis weight of 175 g/m^2 and a thickness of 257 μm was measured in a standard test atmosphere of 23 °C/50% relative humidity (RH). The test procedure consisted of three repetitions of loading-unloading tests, named 1, 2 and 3 accordingly (see Fig. 2 and Table 1). The test samples were initially conditioned at 50% RH. Between the repetitions of the load-unload tests, the board samples were conditioned to 35% and 98% RH levels in a climate chamber (Memmert Climatic CTC 246 MEMMCTC256) that produced changing RH as described in Table 1. The temperature was 23 °C. The relative humidity target levels were chosen according to the climate chamber's user manual in a manner that the levels were in a safe operating region. There were also reference samples which were conditioned at constant 50% RH and 23 °C in the test

ACCEPTED MANUSCRIPT

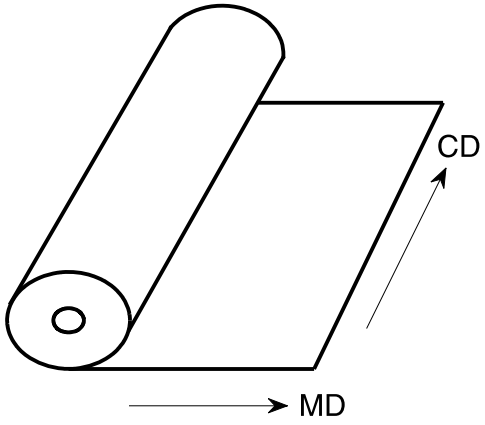

Figure 1: The in-plane directions of paperboard. MD and CD stand for machine and cross-machine direction, respectively.

laboratory for the same time period as that of the samples conditioned in the climate chamber. Tensile tests were performed using a commercial Lloyd Instruments tensile tester equipped with a 100 N (in the preliminary test 1 kN for the MD) load cell. The span length and width of the samples were 180 mm and 15 mm, respectively. The elongation speed was 1 mm/s.

In the preliminary tests, the MD (machine direction) and CD (cross-machine direction) samples were strained until rupture, using a constant elongation speed of 1 mm/s. The flute direction of the corrugated board, which typically carries the main top-load of stacked boxes, is along the CD. Also, the non-linear load-elongation region is more prominent in the CD. Due to those aspects, the CD samples were selected for cyclic tests. The target tension of 6500 N/m (point A in Fig. 2) was fixed according to the preliminary test results of the CD samples.

ACCEPTED MANUSCRIPT

Examples of the measured curves describing the typical tension-strain behavior are presented in Fig. 3. In the measurements four parallel tests were conducted and minor variation between samples was detected. The greatest difference in the curves was obtained between the first and second tensile test. The third load-elongation curve is nearly equivalent to the second one. The difference between the first and subsequent load curves is more notable when the samples have undergone the humidity cycling between the load-elongation tests. Fig. 4 presents the instant strain measured immediately after the tension was released to zero in approximately 3 seconds as well as the

Table 1: The cyclic tensile test procedure for cyclic relative humidity (RH) conditioned samples and reference samples.

Operation: Cyclic RH cond. sample	Time	Operation: Ref. sample
Tensile test 1		Tensile test 1
From 50% RH to 35% RH	6 hours	at 50% RH
From 35% RH to 98% RH	16 hours	at 50% RH
From 98% RH to 50% RH	6 hours	at 50% RH
Tensile test 2		Tensile test 2
at 50% RH	16 hours	at 50% RH
From 50% RH to 35% RH	6 hours	at 50% RH
From 35% RH to 98% RH	16 hours	at 50% RH
From 98% RH to 50% RH	6 hours	at 50% RH
Tensile test 3		Tensile test 3

ACCEPTED MANUSCRIPT

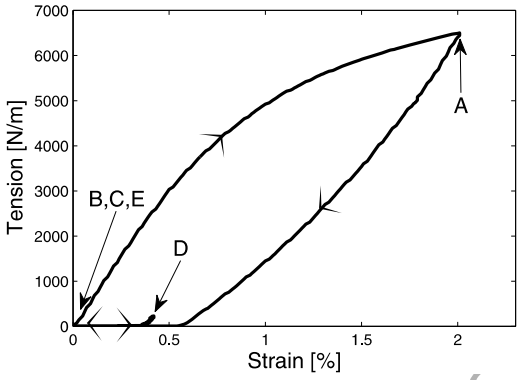

Figure 2: One tensile test. The sample is loaded to the target tension of 6500 N/m (B → A); unloading to the initial start position of the tensile test (A → C); a 30-second pause (C); loading to 200 N/m tension (C → D); and unloading to the initial start position of the tensile test (D → E).

strain measured after about 30 seconds of delayed strain recovery. The strains decrease in consecutive load-elongation tests, but the release of the dried-

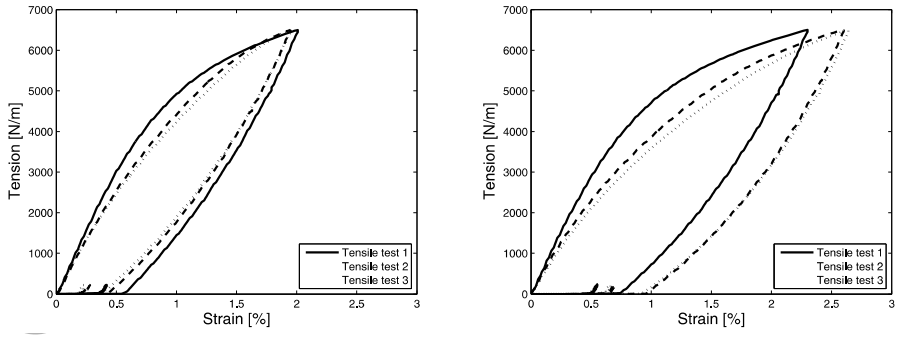

Figure 3: The measured tension-strain curves of one reference sample (left) and of one cyclic RH-conditioned sample (right).

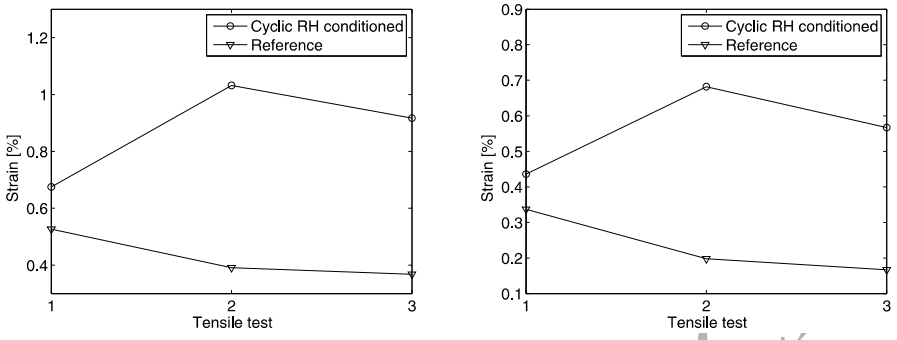

Figure 4: The strain measured instantly at zero tension occurring about 3 seconds after tension release (left), and the strain measured after 30 seconds of strain recovery at zero tension (right).

in strain presumably occurring during the first humidity cycling increases both the instant 3 s strain and the 30 s strain. The important observations concerning hardening modeling in the next section is that an additional set of "permanent" 30 s strain is introduced with consecutive loadings, although the loading was extended to the same maximum tension of 6500 N/m at every repetition.

Examples of fitted tension-strain curves are presented in Fig. 5. The fitting procedure introduced in Erkkilä et al. (2013) includes the determination of the elastic modulus E, the hardening constant H, the yield stress σ_y and the yield strain ε_y. The fitted stress-strain curves follow the equation (Erkkilä et al. (2015))

$$\sigma = \begin{cases} E\varepsilon & \text{if} \quad \varepsilon \leq \varepsilon_y \\ E\varepsilon_y - \frac{H}{2E} + \sqrt{H\left(\frac{H}{4E^2} + \varepsilon - \varepsilon_y\right)} & \text{if} \quad \varepsilon > \varepsilon_y \end{cases} . \tag{1}$$

The fitted material parameters are presented in Fig. 6. The theoretical plastic

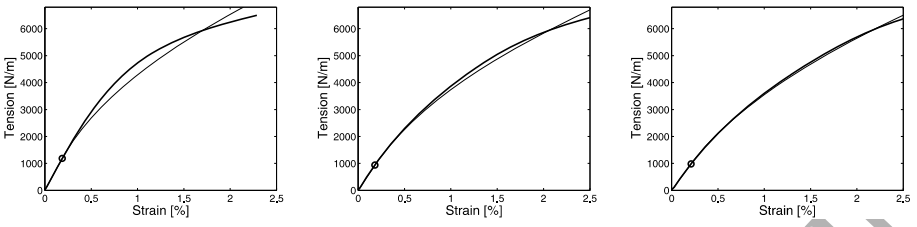

Figure 5: Examples of measured (thick line) and fitted (thin line) tension-strain curves for the RH-cycled samples. On the left is tensile test 1, in the middle is tensile test 2, and on the right is tensile test 3. The fitted yield point is marked with a circle.

strain determined from the fitted curves at a tension of 6500 N/m, using the relation $\varepsilon_p = \varepsilon - \sigma/E$ is presented in Fig. 7. A significant result is that the linear region at the beginning of the load elongation test does not become longer, and the yield stress actually decreases in the repetitions.

3. Material model

Concerning hardening modeling, the most significant observation based on the measurements presented in this work is that in consecutive loading-unloading cycles, the yield stress either stays roughly constant or decreases, and an additional permanent set of strains is obtained even when the maximum tension of repetitions stays constant. The three different hardening approaches are presented in this section.

According to the measured results presented above, the first straining may particularly notably change the shape of the tension-strain curve, and the linear behavior is reduced after the first straining. Indeed, the changes in the material parameters are not profoundly different and relevant for the

comparison of the modeling approaches of this study. In the modeling approach, one stress-strain curve is used for the dry solids content 95% and the dry solids content dependence is obtained from the reference Erkkilä et al. (2015). The stress-strain curves for the maximum and the minimum dry solids contents and the discretization of the curves are illustrated in Fig. 8. In the continuum mechanical model plane stress is assumed, and the yield surface is approximated with the simple von Mises yield function

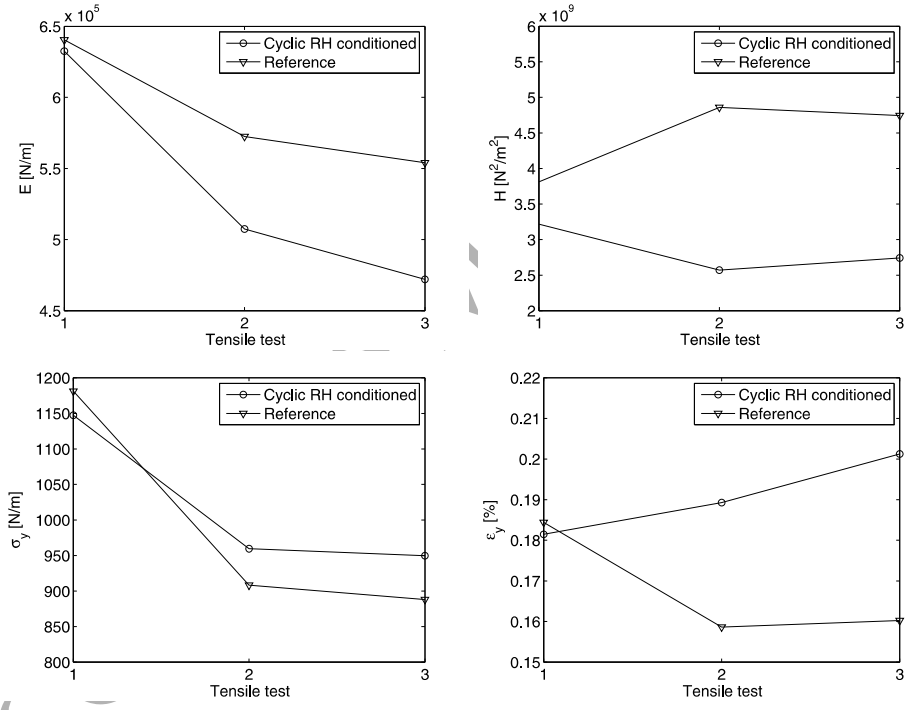

Figure 6: The CD elastic modulus E (upper left), the hardening constant H (upper right), the yield stress σ_y (bottom left) and the yield strain ε_y (bottom right) as a function of the tensile tests. The results are the mean values of four parallel tests.

$$f(\sigma) = \sqrt{\sigma_{11}^2 - \sigma_{11}\sigma_{22} + \sigma_{22}^2 + 3\sigma_{12}^2} \tag{2}$$

where σ_{11}, σ_{22} and σ_{12} are the MD and CD stresses and MD-CD shear stress, respectively. The usage of the von Mises yield function instead of a more sophisticated yield function is based on two factors: 1) in the simulations, all external forces are applied to the CD, and the MD is not externally constrained; and 2) the moisture expansion coefficient in the CD is 3.33 times greater than that in the MD, affecting the CD domination in internal stresses. The moisture expansion coefficients have the measurement-based values $\beta_1 = 0.036$ [%/%] and $\beta_2 = 0.120$ [%/%] for the MD and CD, respectively, and the typical value 0.27 is used for Poisson's ratio μ. The shear modulus G_{12} is approximated according to Gibson (1994) by the equation

$$G_{12} = \frac{E}{2(1+\mu)}. \tag{3}$$

The border between elastic and plastic behavior in the first dry solid content

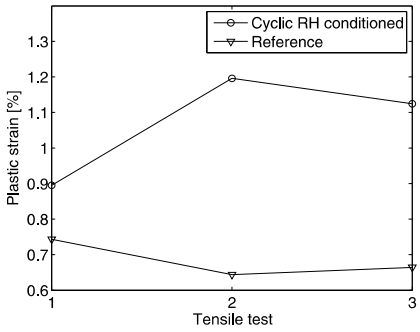

Figure 7: The theoretical plastic CD strain obtained after 6500 N/m of tension. The results are the mean values of the four parallel tests.

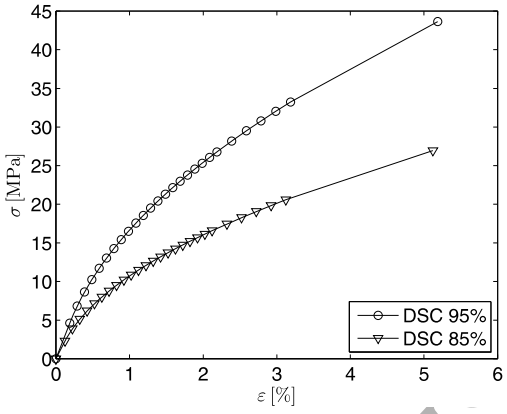

Figure 8: The stress-strain curves used in all cycles for the maximum and the minimum dry solids contents. The first circle and triangle from the origin are the yield points, and the circles and triangles represent the discretization of the stress-strain curves; linear behavior is assumed between the points.

cycle (see Fig. 9) is defined as

$$f(\sigma) = \begin{cases} \sigma_y & \text{if} \quad f(\sigma) \leq \sigma_y \\ \sigma_h & \text{if} \quad f(\sigma) > \sigma_y \end{cases} \tag{4}$$

where

$$\sigma_h = \max\left(E\varepsilon_y - \frac{H}{2E} + \sqrt{H\left(\frac{H}{4E^2} + \varepsilon - \varepsilon_y\right)}\right) \tag{5}$$

and $\sigma_y = 1186$ N/m (4.615 MPa). When a new dry solids content cycle begins, Eq. (4) is reformulated as

$$f(\sigma) = \begin{cases} \sigma_Y & \text{if} \quad f(\sigma) \leq \sigma_Y \\ \sigma_h & \text{if} \quad f(\sigma) > \sigma_Y \end{cases} \tag{6}$$

where σ_Y: $\sigma_y \leq \sigma_Y \leq \sigma_h$ is the new yield stress, depending on the approach. Three different approaches are investigated:

- *Approach 1*: In Eq. (6) $\sigma_Y = \sigma_h$ i.e. isotropic hardening behavior is assumed throughout the simulation.

- *Approach 2*: The internal stresses σ_{int} are set to zero between the dry solids content cycles and in Eq. (6) $\sigma_Y = \sigma_y$. σ_{int} are the stresses induced by the through-thickness variation of the plastic strains after the dry solids content cycle.

- *Approach 3*: The internal stresses are not set to zero between the dry solids content cycles and (due to that) in Eq. (6) $\sigma_Y = \sigma_y + \sigma_{int}$ or when external stress σ_{ext} is included $\sigma_Y = \sigma_y + \sigma_{int} + \sigma_{ext}$.

Approach 1 is a reference case and Approaches 2 and 3 correspond to the different "relaxation" of the internal stresses between the dry solids content cycles. In approach 2 all internal stresses are relaxed between the cycles

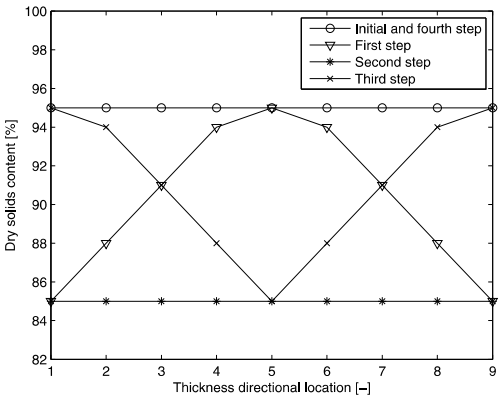

Figure 9: The through-thickness dry solids content distributions of one cycle. Locations 1 and 9 are the surface layers, whereas location 5 is the mid-point of the through-thickness direction.

ACCEPTED MANUSCRIPT

whereas in Approach 3 the internal stresses in the end of the cycle remain to the next dry solids content cycle.

4. The numerical simulations

The numerical results were obtained with the finite element method using the commercial software ABAQUS/Standard. The element employed was shell element S4R with a composite structure (see ABAQUS (2013)). In the thickness direction, the element was partitioned into eight layers of equal thickness (see Fig. 10). The in-plane size of the sample was 100 mm in both the MD and CD, and the thickness was 0.257 mm. The boundary conditions were allowing for free in-plane displacements in both the MD and CD. All six degrees of freedom were constrained in the middle node of the mesh, and the out-of-plane displacements and the rotations were set to zero at the edges of the mesh. The boundary conditions used represent only one potential approach; the same results could also be obtained with other suitable boundary conditions. No out-of-plane deformations occurred due to the homogeneous structure of the sample and to the symmetric dry solids content distributions (see Fig. 9).

The development of dry solids content distributions in paper and paperboard has been studied by multiple authors (e.g. Lavrykov et al. (2004), Dano and Bourque (2009), Östlund (2006) and Baggerud and Stenström (2005)). For the purposes of this paper, one dry solids content cycle is defined by the initial situation and four simulation steps. The through-thickness dry solids content distributions are thus defined as follows:

1. Step 0: The initial situation: A constant dry solids content with a

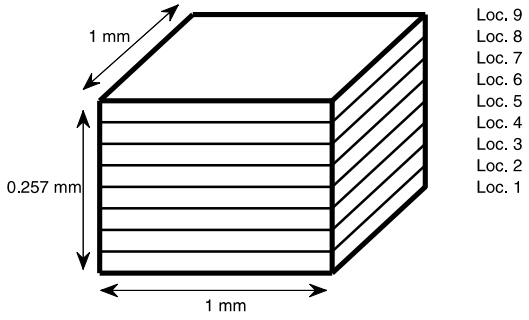

Figure 10: The element used in the simulations with nine thickness directional locations where the dry solids content is given.

through-thickness of 95%.

2. Step 1: In the outer surfaces of the paperboard, the dry solids content is decreased to 85%, while in between the middle layers, the dry solids content remains at 95%.
3. Step 2: A constant dry solids content with a through-thickness of 85%.
4. Step 3: In the outer surfaces of the paperboard, the dry solids content is increased to 95%, while between the middle layers, the dry solids content remains at 85%.
5. Step 4: A constant dry solids content with a through-thickness of 95%. This is the initial situation for the next cycle.

The dry solids content change is applied linearly over one step; see Fig. 11.

Fig. 12 displays the CD plastic strains and the final strains of the three different approaches, described as follows. In Approach 1, the isotropic hardening behavior is used throughout the simulation. In Approach 2, the yield point is the same in the beginning of every dry solids content cycle, and

ACCEPTED MANUSCRIPT

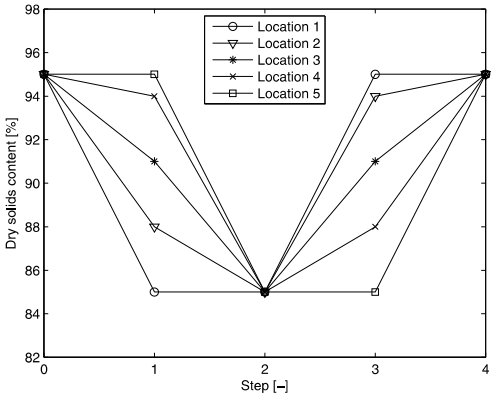

Figure 11: The dry solids contents of the through-thickness locations during the steps constituting one cycle. Step 0 presents the initial situation, and because of symmetry, only locations 1 to 5 are presented.

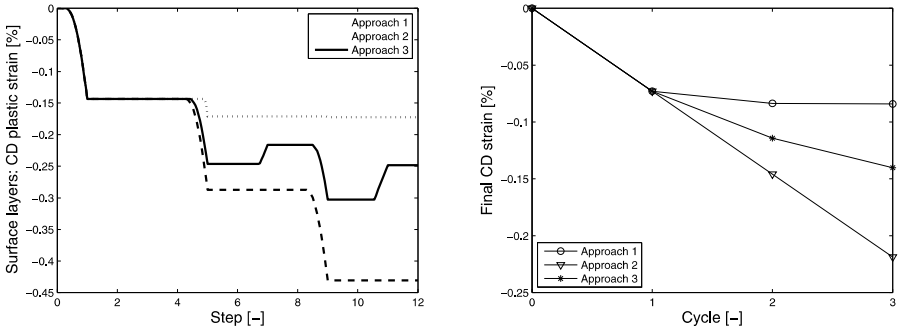

Figure 12: The CD plastic strain of the surface layers (left) and the final CD strains following the cycles (right). In the latter, the lines between the markers are used only for clarity. The four steps constitute one dry solids content cycle. No external tensions are applied to the sample.

ACCEPTED MANUSCRIPT

the internal stresses are adjusted to zero between the cycles. Now simple results for the plastic strains and the final strains may be obtained: the plastic strain behaves in the same way in every cycle and the final strain increases linearly. In Approach 3, the yield point in the beginning of every dry solids content cycle is defined by the final internal stresses of the preceding dry solids content cycle; the behavior arises from the stress transfer between the cycles. This is supported by Östlund et al. (2004), as their work demonstrates that the internal stresses generated during the drying process with through-thickness dry solids content gradients are not relaxed by the dry solids content cycling. With Approach 3, the increment in the plastic and final strains decreases as the number of cycles increases. The strain appears to asymptotically approach some constant strain. The results share some common features with the irreversible behavior of hygroexpansion; see, for example, Nanri and Uesaka (1993). The largest irreversible shrinkage is obtained in the first exposure to the lower dry solids content, and smaller irreversible shrinkages may be obtained in subsequent exposures.

Fig. 13 presents the internal residual stresses occurring after the dry solid content cycles. The shape of the obtained stress profile arising from cyclic DSC changes is more complicated than that resulting from a single drying process with a through-thickness dry solids content gradient (see e.g. Östlund et al. (2004) and Erkkilä et al. (2015)): layers 2, 3, 6 and 7 are under compressive stress, while the surface layers (1 and 8) and the middle layers (4 and 5) are under tensile stress. The overall level of the internal stresses are in the vicinity of the internal stresses obtained by Östlund et al. (2004).

Fig. 14 presents how external compression affects the CD plastic strains

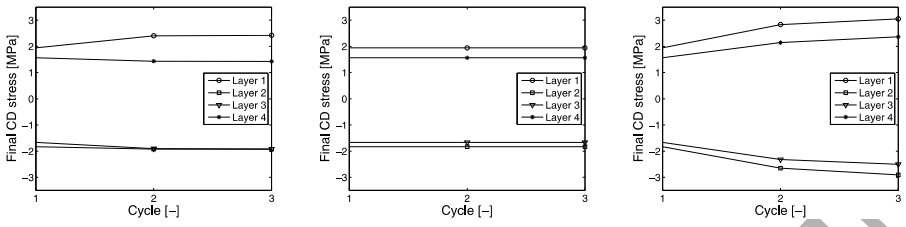

Figure 13: Residual stresses after the dry solid content cycles. For Approach 2 (middle), the constant stresses are obtained, while in Approaches 1 (left) and 3 (right), the stresses are affected by the number of cycles. Because of symmetry, only layers 1 to 4 are presented.

and the final CD strains in the case of Approach 3. The level of external compression has a significant effect on the slopes in the final CD strains, so with increased external compression, more cycles are needed to approach the constant asymptotic value for the final CD strain. In Strömbro and Gud-

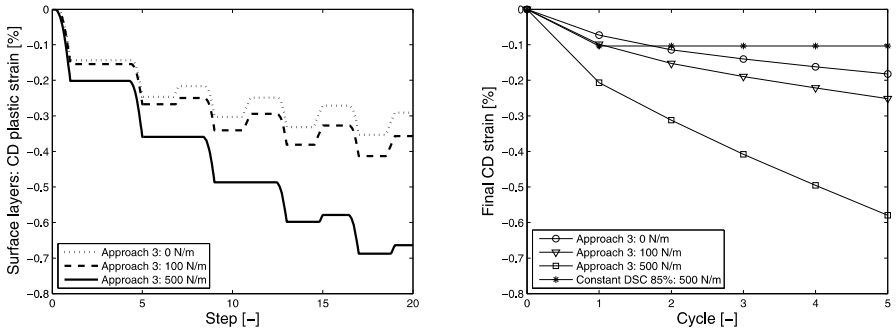

Figure 14: The CD plastic strain of the surface layers (left), and the final CD strains following the cycles (right). In the latter, the lines between the markers are used only for clarity, and the case of 500 N/m external compression without the dry solids content cycles is added as a reference.

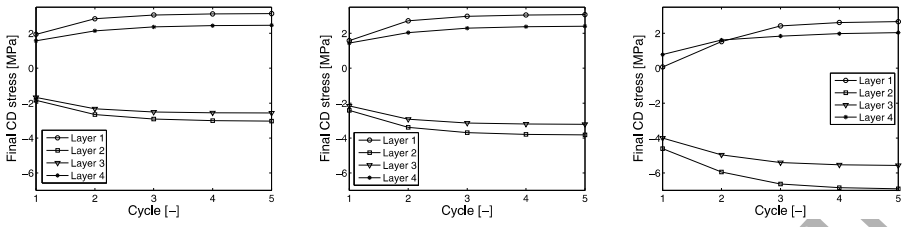

Figure 15: The residual stresses after the dry solid content cycles performed with three different levels of external tensions: 0 N/m (left), 100 N/m (middle), and 500 N/m (right). Because of symmetry, only layers 1 to 4 are presented.

mundson (2008b), the mechano-sorptive creep curves were measured using external compression of six different forces, ranging from -1.6 kNm/kg to -4.7 kNm/kg. Concerning the simulation results of this work using 500 N/m = 2.86 kNm/kg of compression, clear similarities to the measured results obtained by Strömbro and Gudmundson (2008b) can be observed, even though the material and DSC cycles are not identical.

Fig. 15 shows how the external tensions impact the residual stresses. The results indicate that the residual stresses after the DSC cycles are altered in a more complicated way than by a shift based on any simple dependence on the external tension (100 N/m: -0.389 MPa and 500 N/m: -1.946 MPa).

5. Conclusions

The loading-unloading tests repeatedly executed with the same test sample strips demonstrated that the most notable difference in the stress-strain curves occurs between the first and second loading. The cyclic conditioning at different relative humidity levels released internal dried-in stresses and

ACCEPTED MANUSCRIPT

changed the stress-strain curve more notably. The theoretical plastic strains determined from the fitted stress-strain curves were higher than the strain measured instantly after the unloading. The correlation between these strains was high, however, and the lower values of the measured instant strain can at least be partly explained by the ca. 3-second time of stress relaxation before the strain measurement could actually be obtained, during which time, besides the elastic recovery, some delayed strain recovery occurs. Even though there were some differences between the material parameters obtained in the fitting of the consecutive stress-strain curves, these differences were not considered significant concerning the capturing of the major trends of the cyclic behavior, and a single material model was chosen to be applied in the simulation approach.

The rheological properties of paper or board are often simulated using viscoelastic models with time-dependent parameters, which is the obvious choice for many contexts, such as that of creep. Multiple studies have measured and found that ambient humidity and moisture content changes accelerate the creep process or induce a release of dried-in stresses. The starting point in the simulations, i.e. the through-thickness dry solids content distributions, is not new; the same basic idea in the case of moisture-accelerated creep has already been discussed by Habeger and Coffin (2000). It has also been shown that in-plane or through-thickness differences of dry solids content can build up internal stresses and plastic-strain differences in samples (Erkkilä et al. (2015)). These observations imply that elasto-plastic simulations might offer a useful viewpoint on cyclic and irreversible straining phenomena. However, the lack of the internal stress relaxation has to be kept on mind when

ACCEPTED MANUSCRIPT

elasto-plastic approaches are used.

The commonly used isotropic elasto-plastic hardening model is not optimized for all approaches, including the several repeated load-unload situations described in this paper. In this paper, the effects of three different hardening approaches on the permanent strain and internal stresses of paperboard were simulated. Approach 3, in which the internal stresses are retained for the next cycle, yielded results which were the most comparable to those of earlier studies (Strömbro and Gudmundson (2008b)).

Acknowledgements

Simulations were performed by ABAQUS commercial software, which was licensed to CSC (the Finnish IT Center for Science).

References

ABAQUS, 2013. ABAQUS Documentation. Dassault Systèmes, Providence, RI, USA.

Alfthan, J., Gudmundson, P., Östlund, S., 2002. A micro-mechanical model for mechano-sorptive creep in paper. Journal of Pulp and Paper Science 28(3), 98-104.

Alfthan, J., 2003. A simplified network model for mechano-sorptive creep in paper. Journal of Pulp and Paper Science 29(7), 228-234.

Alfthan, J., 2004. The effect of humidity cycle amplitude on accelerated tensile creep of paper. Mechanics of Time-Dependent Materials 8(4), 289-302.

ACCEPTED MANUSCRIPT

Allaoui, S., Aboura, Z., Benzeggagh, M.L., 2009. Phenomena governing uniaxial tensile behavior of paperboard and corrugated cardboard. Composite Structures 87, 80-92.

Baggerud, E., Stenström, S., 2005. Further insight in the web consolidation process, Part III: Modelling of paper shrinkage. Nordic Pulp and Paper Research Journal 20(1), 58-63.

Borgqvist, E., Lindström, T., Tryding, J., Wallin, M., Ristinmaa, M., 2014. Distortional hardening plasticity for paperboard. International Journal of Solids and Structures 51, 2411-2423.

Byrd, V.L., Koning, J.W., 1978. Edgewise compression creep in cyclic relative humidity environments. Tappi 61(6), 35-37.

Castro, J., Ostoja-Starzewski, M., 2003. Elasto-plasticity of paper. International Journal of Plasticity 19, 2083-2098.

Coffin, D., 2005. The creep response of paper, in: Proceedings of 13th Pulp and Paper Fundamental Research Symposium, Cambridge, pp. 651-747.

Coffin, D., 2009. Developing a deeper understanding of the constitutive behavior of paper, in: Proceedings of 14th Pulp and Paper Fundamental Research Symposium, Oxford, pp. 841-875.

Coffin, D., 2012. Use of the efficiency factor to account for previous straining on the tensile behavior of paper. Nordic Pulp and Paper Research Journal 27(2), 305-312.

ACCEPTED MANUSCRIPT

Craven, B.D., 1962. Stress relaxation and work hardening in paper. Appita Journal 16(2), 57-70.

Dano, M.-L., Bourque, J.-P., 2009. Deformation behavior of paper and board subjected to moisture diffusion. International Journal of Solids and Structures 46, 1305-1316.

Erkkilä, A.-L., Leppänen, T., Hämäläinen, J., 2013. Empirical plasticity models applied for paper sheets having different anisotropy and dry solids content levels. International Journal of Solids and Structures 50, 2151-2179.

Erkkilä, A.-L., Leppänen, T., Hämäläinen, J., Tuovinen, T., 2015. Hygro-elasto-plastic model for planar orthotropic material. International Journal of Solids and Structures 62, 66-80.

Gates, E.R., Kenworthy, I.C., 1963. Effects of drying shrinkage and fibre orientation on some physical properties of paper. Paper Technology 4(5), 485-493.

Gibson, R.F., 1994. Principles of Composite Material Mechanics. McGraw-Hill Inc.

Guo, Y., Fu, Y., Zhang, W., 2007. Creep properties and recoverability of double-wall corrugated paperboard. Experimental Mechanics 48, 327-333.

Habeger, C., Coffin, D., 2000. The role of stress concentrations in accelerated creep and sorption-induced physical aging. Journal of Pulp and Paper Science 26(4), 145-157.

ACCEPTED MANUSCRIPT

Haslach H.W. Jr., 1994. The mechanics of moisture accelerated tensile creep in paper. Tappi Journal 77(10), 179-186.

Lavrykov, S., Ramarao, B.V., Lyne, Å.L., 2004. The planar transient hygroexpansion of copy paper: experiments and analysis. Nordic Pulp and Paper Research Journal 19(2), 183-190.

Leake, C., Wojcik, R., 1992. Humidity cycling rates: How they affect container life spans, in Proceedings, Cyclic Humidity Effects on Paperboard Packaging, Forest Products Laboratory, Madison, WI, pp. 134-144.

Lif, J.O., 2006. Hygro-viscoelastic stress analysis in paper web offset printing. Finite Elements in Analysis and Design 42(5), 341-366.

Lipponen, P., Leppänen, T., Kouko, J., Hämäläinen, J., 2008b. Elasto-plastic approach for paper cockling phenomenon: on the importance of moisture gradient. International Journal of Solids and Structures 45, 3596-3609.

Mäkelä, P., Östlund, S., 2003. Orthotropic elastic-plastic material model for paper materials. International Journal of Solids and Structures 40, 5599-5620.

Nanri, Y., Uesaka, T., 1993. Dimensional stability of mechanical pulps - drying shrinkage and hygroexpansivity. Tappi Journal 76(6), 62-66.

Padanyi, Z.V., 1991. Mechano-sorptive effects and accelerated creep in paper, in: Proceedings of International Paper Physics Conference, Kona, Hawaii, pp. 397-411.

ACCEPTED MANUSCRIPT

Padanyi, Z.V., 1993. Physical aging and glass transition: effects on the mechanical properties of paper and board, in: Proceedings of 10th Pulp and Paper Fundamental Research Symposium, Oxford, pp. 521-545.

Reichel, S., Kaliske, M., 2015. Hygro-mechanically coupled modelling of creep in wooden structures, Part I: Mechanics. International Journal of Solids and Structures 77, 28-44.

Reichel, S., Kaliske, M., 2015. Hygro-mechanically coupled modelling of creep in wooden structures, Part II: Influence of moisture content. International Journal of Solids and Structures 77, 45-64.

Selway, J.W., Kirkpatrick, J., 1992. The assessment of high humidity corrugated box performance, in Proceedings, Cyclic Humidity Effects on Paperboard Packaging, Forest Products Laboratory, Madison, WI, pp. 31-47.

Skowronski, J., Robertson, A.A., 1986. The deformation properties of paper: Tensile strain and recovery. Journal of Pulp and Paper Science 12(1), 20-25.

Strömbro, J., Gudmundson, P., 2008a. Mechano-sorptive creep under compressive loading - A micromechanical model. International Journal of Solids and Structures 45, 2420-2450.

Strömbro, J., Gudmundson, P., 2008b. An anisotropic fibre-network model for mechano-sorptive creep in paper. International Journal of Solids and Structures 45, 5765-5787.

Uesaka, T., Kodaka, I., Okushima, S., Fukuchi, R., 1989. History-dependent dimensional stability of paper. Rheologica Acta 28, 238-245.

ACCEPTED MANUSCRIPT

Uesaka, T., Moss, C., Nanri, Y., 1992. The characterisation of hygroexpansivity of paper. Journal of Pulp and Paper Science 18(1), 11-16.

Urbanik, T.J., 1995. Hygroexpansion-creep model for corrugated fiberboard. Wood and Fiber Science 27(2), 134-140.

Vlahinić, I., Thomas, J.J., Jennings, H.M. Andrade, J.E., 2012. Transient creep effects and the lubricating power of water in materials ranging from paper to concrete and Kevlar. Journal of the Mechanics and Physics of Solids 60, 1350-1362.

Xia, Q.S., Boyce, M.C., Parks, D.M., 2002. A constitutive model for the anisotropic elastic-plastic deformation of paper and paperboard. International Journal of Solids and Structures 39, 4053-4071.

Östlund, M., Östlund, S., Carlsson, L.A., Fellers, C., 2004. The influence of drying restraints and beating degree on residual stress build-up in paperboard. Journal of Pulp and Paper Science 30(11), 289-292.

Östlund, M., 2006. Modeling the influence of drying conditions on the stress buildup during drying of paperboard. Journal of Engineering Materials and Technology, Transactions of the ASME 128(4), 495-502.

ACCEPTED MANUSCRIPT